Study of precipitant systems by computerised simulation. Influence of optical elements on the noise associated with the transmittance

J.A. Poce-Fatou *, R. Alcántara, J. Martín

Departamento de Química Física, Facultad de Ciencias, Universidad de Cadiz, Apartado de Correos 40, 11510 Puerto Real (Cádiz), Spain

Abstract

The transmittance signal of a precipitant system measured with a focused laser beam carries associated noise coming from several sources. In this work, we have studied the influence of the focal parameters (wavelength, focal length and prefocused radius of the beam) on the maximum noise reached in equivalent nucleation processes. For this purpose, a simulation program of precipitating systems, designed in FORTRAN 90, has been developed. The program generates simulated transmittances, which are processed by another computer program to extract associated noise. Wide ranges of values of the focal parameters have been analysed, finding relationships between the maximum noise and the focal parameters. They have been justified in connection with the changes observed in the radial parameters, which define the size and shape of the focused path. © 2001 Elsevier Science Ltd. All rights reserved.

Keywords: Precipitation; Noise; Transmittance; Simulation; Wavelength; Laser

1. Introduction

The uncertainty inherent in every experimental measurement can be caused by various factors among which we can mention those caused by the performance of the instrumentation, imperfections of the experimental design, changes undergone by the physical chemical parameters of the system, etc. We use the term noise to refer to all the deviations detected between the exact and the experimental values.

The presence of noise in the measurement of experimental data is usually a distorting factor. However, in a recent study about precipitant systems (Poce-Fatou et al., 2000), we have found that the noise associated with the transmittance measured using a focused laser beam could be related to physical chemical properties of the process. More specifically, it could be related to the number, morphology and size of the precipitated particles, as well as to the relative influence of the nucleation and growth processes.

The size of the beam inside the precipitant system is as small as the particles and this converts the beam into a probe capable of detecting their presence (Martín et al., 1991, 1992). The parameters that determine the dimensions of the focal region are the wavelength of the radiation, the focal length of the lens and the prefocused radius of the beam. The use of different values for these magnitudes in different tests could be useful for evaluating their influence on the associated noise. However, the dynamic properties of the precipitant systems must also be taken into account.

* Corresponding author. Tel.: + 34-956-016178; fax: + 34-956-016288.

E-mail address: juanantonio.poce@uca.es (J.A. Poce-Fatou).
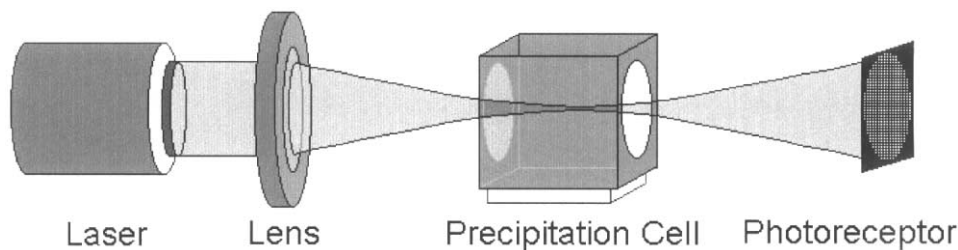
Fig. 1. Disposition of elements in the virtual device that has been used as basic optical scheme in the simulated precipitation processes.

The evolution of the particles can be very different in terms of size, number and morphology, even in similar tests carried out under the same experimental conditions.

This adds new sources to the noise, which are very difficult to control. To avoid these sources, we have developed a model of precipitant systems using a computer simulation technique, which allows control of the parameters related to the dynamic behaviour of the system. This technique has been used to characterise the influence of the optical parameters (wavelength of the radiation, focal length of the lens and prefocused radius of the beam) on the noise associated with the transmittance.

2. Materials and methods

2.1. General description of the simulation program

The program used in this work has been designed in FORTRAN 90[1]. It is used for simulating experiments where both the main features of the precipitant system and the radiation used as an optical probe can be defined independently.

The simulated equipment is based on that used to obtain experimental results in a recent study (Poce-Fatou et al., 2000). In the tests carried out with that equipment, precipitated particles were generated using an injection technique where an inducing solution was added to a base solution. Concentrations of both solutions were sufficiently high, so that the ionic concentration product (ICP) was widely exceeded when they came into contact, thus favouring the generation of new nuclei of the precipitate against the growth of the initial ones. Then, the precipitated particles were kept in suspension with a magnetic stirrer.

As in the experimental tests, the precipitation process is simulated inside a cubic volume according to the basic optical scheme shown in Fig. 1. The focused path

corresponds to a hyperbolic function inscribed inside the cube with its propagation axis arranged perpendicularly to opposite faces of the cube.

The evolution of the process is carried out with additions of small amounts of precipitated mass, d_m, along N stages, until the final mass value, m_f, is reached. In each stage, the program uses the added mass to generate new particles of volume V_p, which are placed in random positions together with those generated in previous stages. In this way, the simulation process is based on pure nucleation, where every particle takes a new position in every new stage.

Under these conditions, some particles may shadow the virtual photoreceptor unit, placed at a right angle in relation to the propagation pathway. The program evaluates the global projection effect, calculating a transmittance value together with data of mass and number of particles, and these are all included in a result file.

Fig. 2 shows the flowchart of the simulation program, which is structured in three main parts,

- simulation of the precipitant system
- simulation of the focused path
- simulation of the photoreceptor unit.

Each of these parts is explained in the following sections, including notes about the conventions and the calculations made to obtain simulated transmittances.

2.2. Simulation of the precipitant system

The simulation program has been designed to control the fluctuations of the noise associated with the transmittance signal which are related to the dynamics of the process. In order to avoid possible morphological influences, only spherical particles have been simulated, so that the surface projected by particles blocking the beam always has a round shape.

In order to avoid the influence of the presence of a wide variety of sizes, the particles have been simulated assuming a unimodal distribution of volumes.

In addition to this, the program works with other considerations, related to the medium in which the precipitation process takes place.
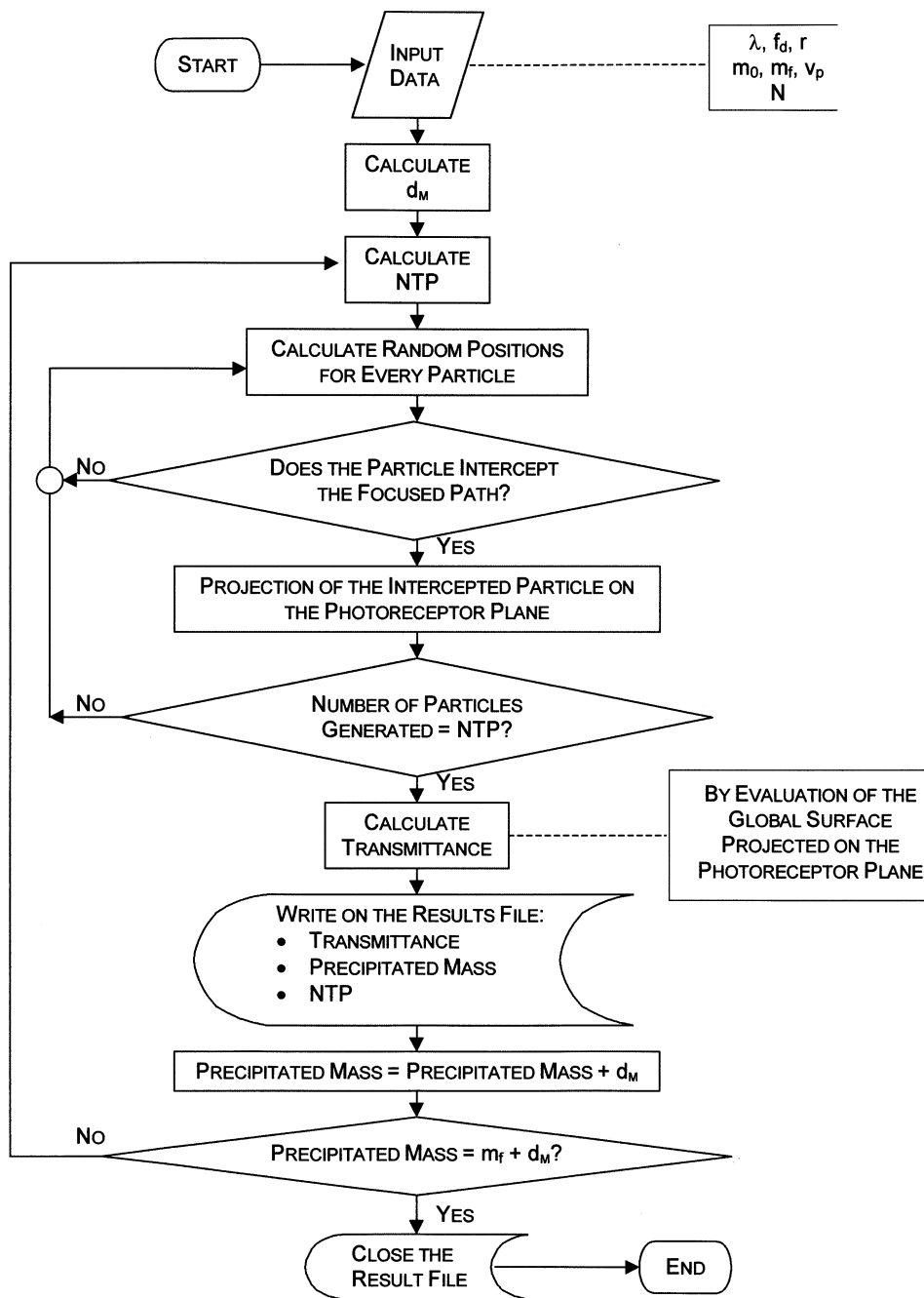
Fig. 2. Flowchart for the program of simulated precipitation processes.

- Just like that used in the experimental device, the virtual precipitation cell is a 40000 μm inner edge cube, totally transparent to laser radiation.
- The positions of all particles are calculated by means of random numbers limited within the dimensions of the precipitation cell.

- Local variations in the refractive index of the liquid medium in which particles are suspended are not considered.
- The precipitated particles have a radiation absorption coefficient of 100% and optical dispersion phenomena are ignored.

2.3. Simulation of the focused path

When the parallel rays of a laser beam cross a convex lens (Gerrard & Burch, 1994), they acquire curvature spreading in accordance with

$$R = \pm\ R_0\sqrt{1+\left(\frac{\lambda y}{\pi R_0^2}\right)^2} \tag{1}$$

Where λ is the wavelength of the radiation, y is the position coordinate along the propagation axis, R is the Gaussian radius of the circular cross-section given by the coordinate y, R_0 is the Gaussian radius of the circular cross-section at the focus, where $y = 0$. R_0 can be calculated by

$$R_0 = \frac{\lambda f_d}{\pi r} \tag{2}$$

Where f_d is the focal length of the lens, r is the Gaussian radius of the prefocused laser beam.

The surface shadowed by a particle eclipsing a cylindrical path is independent of its position and can be calculated as an orthogonal projection. However, the program simulates a focused path where there is an evident relationship between the position where the particle intercepts the beam and the projected surface.

The program calculates the size the intercepted particle would have in a cylindrical path equivalent to the focused one, and then it evaluates the orthogonal projection surface.

The size of the particle in this path depends on the relationship between R_i and R_f, where R_i is the radius of the circular cross-section of the focused path at the intercepting position, R_f is the radius of the circular cross-section of the focused path on the photoreceptor plane.

Fig. 3 shows an R_p radius particle placed in a focused path, projecting a round shape surface of radius R_T on the photoreceptor plane. If R_i is the radius of the cross-section of the focused path at the intercepting position, the area of the orthogonal projection is calculated as that of a circle of radius $R'_p = R_T$, placed inside an equivalent cylindrical path. This value can be calculated as shown below,

$$R'_p = R_T = R_p\frac{R_i}{R_f} \tag{3}$$

2.4. Simulation of the photoreceptor unit

In order to simulate the virtual photoreceptor, a bidimensional matrix of 501×501 units has been defined. Inside this matrix, the photoreceptor consists of an internal circular selection with a radius of 250 units that contains numerical information in the form of zeros (0) and ones (1).

In the simulated device, the virtual photoreceptor stands orthogonally with the propagation axis, receiving the beam coming out from the precipitation cell, at 20000 μm of its geometrical centre. At this point, the circular cross-section of the focused path reaches its largest size and its value depends on the focal parameters λ, f_d and r.

Before the generation of any particle, the initial situation on the photoreceptor unit fits with that of a matrix containing null values (0) at every position. In the course of the precipitation process, particles blocking the beam generate circular projections in a wide range of sizes. The effect of these particles on the photoreceptor plane is registered assigning a value equal to one (1) to the positions projected on the matrix.

The sum of the whole of the matrix positions in every stage describes the transmittance evolution in terms of projected surfaces, and can be calculated by

$$\text{Transmittance} = \frac{N-\sum\limits_{i=1}^{N}X_i}{N}\times 100 \tag{4}$$

Where N is the number of positions inside the 250 unit radius circular matrix, X_i is the numerical value (0 or 1) assigned to the ith matrix position.

In Fig. 4, a transmittance curve of a virtual precipitation process is shown. The noise associated with the
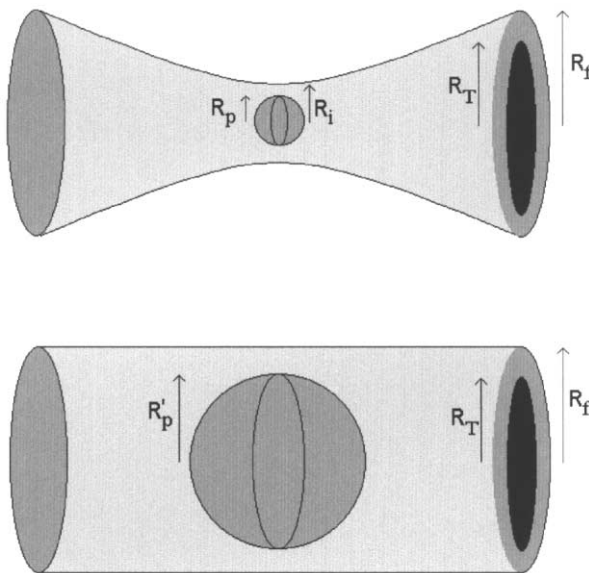
Fig. 3. A spherical particle of radius R_p is placed in a position where the circular cross-section of a focused path has a radius equal to R_i. This particle projects a round shape surface of radius R_T over a round shape photoreceptor plane with a radius R_f. In an equivalent cylindrical path, a particle of radius R'_p generates the same surface over the same photoreceptor plane.
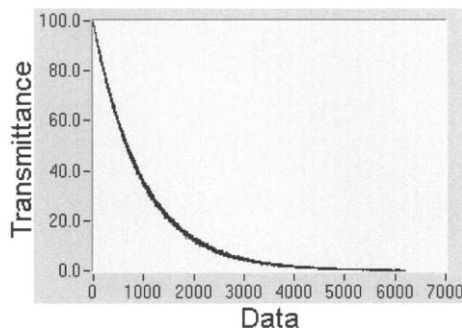
Fig. 4. Sample of a plot generated by the simulation program using $\lambda = 632.8$ nm, $r = 400$ μm and $f_d = 20$ cm.

transmittance data was calculated with another computer program, designed in LABVIEW™ 5.0[2]. The program works with a subset of an odd number of consecutive data (C) that shifts along all the data set, calculating in every movement the best third-order polynomial fit.

Finally, the noise associated with the averaged transmittance of the subset is calculated by means of the mean squared error parameter, given by

$$\text{Noise} = \sqrt{\frac{1}{(ne - ns)}\sum_{ns}^{ne}(TE_i - TC_i)^2} \qquad (5)$$

Where ns and ne are the numerical positions of the initial and final data in the subset of evaluated transmittances, TE_i is the ith experimental transmittance value, and TC_i is the ith transmittance value averaged with the best third-order polynomial fit.

As the subset shifts forward, the program generates results of noise and averaged transmittances.

3. Results and discussion

Next, we set forth the results of the analysis of the influence of the focal parameters, λ, f_d and r, on the noise associated with the transmittance signal, obtained by performing three series of 20 simulations in which a wide range of values have been evaluated.

The precipitation processes were divided into 6195 stages where a constant amount of precipitated mass, d_m, was added and used for the generation of more new particles of constant volume, V_p.

The data of transmittances generated in every simulation were similar to those shown in Fig. 4. These were later processed by the program for calculating noise,

Table 1
Common parameters used in all the simulated processes performed to evaluate the influence of λ, f_d and r on the noise associated with the transmittance

Number of stages (N)	6195
Initial precipitated mass (M_0/mg)	0.05
Final precipitated mass (M_f/mg)	35
Mass added in every stage (d_m/μg)	5.64
Particle volume (V_p/μm^3)	50
Particle radius (R_p/μm)	2.29
Initial number of particles (N_0)	10^6
Final number of particles (N_f)	7×10^8

using a subset of 151 data. The results of this second processing generated graphs similar to that shown in Fig. 5. Common data used in all the simulations are listed in Table 1.

3.1. Influence of the wavelength, λ

The values of the parameters used in the simulations for analysing the influence of the wavelength are listed below.

Range of evaluated wavelengths (λ/nm)	460–650
Focal length (f_d/cm)	10
Prefocused radius (r/μm)	400

The evaluated range of this parameter covers almost the whole of the visible spectrum. The parameters f_d and r have been kept constant, defining a value of 400 μm for the latter which coincides with typical data of commercial lasers.

All curves of associated noise versus averaged transmittance showed a trace similar to that of the curve of Fig. 5 but with significant discrepancies in the magnitudes. In order to remove small fluctuations, every graph was fit to the best fifth-order polynomial, and then analysed by another computer program designed
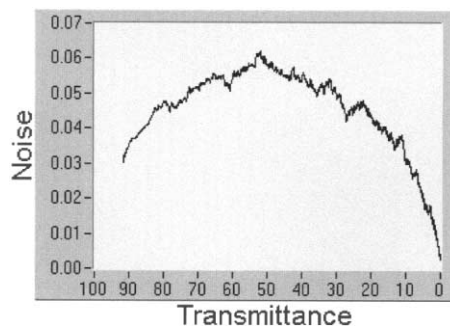
Fig. 5. Plot of associated noise versus transmittance calculated from the sample shown in Fig. 4 using $\lambda = 632.8$ nm, $r = 400$ μm and $f_d = 20$ cm.

---

[2] National Instruments™. © Copyright 1998. This programming language was chosen because it has proper modules that make programming this kind of application easier and faster.

Table 2
Transmittances (T_M) and associated noise (N_M) corresponding to the points of maximum noise reached in the simulated processes performed to evaluate the influence of λ. These points have been calculated using the best fifth-order polynomial fit. The radius of the focus (R_0) and the radius of the path at the photoreceptor plane (R_f) are also shown

λ/nm	460	470	480	490	500	510	520	530	540	550
N_M/%	0.152	0.142	0.146	0.134	0.135	0.143	0.138	0.138	0.132	0.129
T_M/%	52.41	52.62	58.15	53.51	56.62	55.54	54.91	58.61	54.63	56.42
R_0/μm	36.61	37.40	38.20	38.99	39.79	40.58	41.38	42.18	42.97	43.77
R_f/μm	87.97	88.31	88.65	89.00	89.35	89.71	90.07	90.43	90.81	91.19
λ/nm	560	570	580	590	600	610	620	630	640	650
N_M/%	0.129	0.124	0.120	0.116	0.119	0.116	0.117	0.113	0.110	0.103
T_M/%	61.03	53.13	48.49	47.23	61.92	55.72	60.62	57.83	58.81	56.87
R_0/μm	44.56	45.36	46.15	46.95	47.75	48.54	49.34	50.13	50.93	51.73
R_f/μm	91.58	91.96	92.36	92.76	93.16	93.58	93.99	94.41	94.83	95.26

in FORTRAN 90 which calculated the position of the maximum, using a method based on Bolzano's theorem (Apostol, 1967) with an accuracy of less than 10^{-6}.

The data that characterise the positions of the maxima are listed in Table 2, together with the radial parameters of the focused path, R_0 and R_f. Fig. 6 shows the variations of these parameters in relation to the value of λ.

It can be seen from Fig. 6A that the maximum noise is in good accord with a linear relationship to λ, where the slope is -2.182×10^{-4}, the intercept is 0.2490 and the correlation coefficient (r^2) is equal to 0.9317. However, Fig. 6B shows that transmittances are in disarray and do not seem to confirm to a mathematical relation.

3.2. Influence of the focal length, f_d

The values of the focal parameters used for analysing the influence of the focal length are shown next.

Wavelength (λ/nm)	632.8
Range of evaluated focal lengths (f_d/cm)	3–22
Prefocused radius (r/μm)	400

The wavelength has been kept constant at 632.8 nm throughout the simulation tests carried out, since that is the typical value of a standard He–Ne laser, an inexpensive device that could be used in future experimental reproductions of the tests.

A summary of the results is given in Table 3, together with the values of the focal parameters R_0 and R_f. Fig. 7 shows the variations of these data in relation to f_d. It can be seen that, as the focal length increases, the maximum noise becomes smaller, following a mathematical relation that can be fit to the exponential function given by

$$y = \frac{A_1 - A_2}{1 + e^{(x - x_0)/dx}} + A_2 \qquad (6)$$
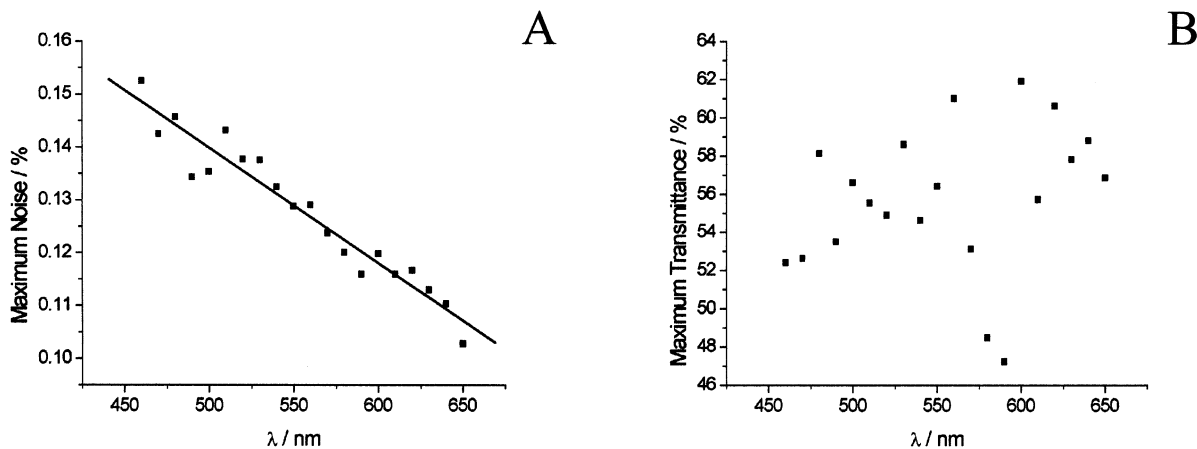
Fig. 6. Plots of data corresponding to the maximum noise reached in the tests for the study of the influence of λ: A, maximum noise versus λ; B, maximum transmittance versus λ.

Table 3
Transmittances (T_M) and associated noise (N_M) corresponding to the points of maximum noise reached in the simulated processes performed to evaluate the influence of f_d. These points have been calculated using the best fifth-order polynomial fit. The radius of the focus (R_0) and the radius of the path at the photoreceptor plane (R_f) are also shown

f_d/cm	3	4	5	6	7	8	9	10	11	12
N_M/%	0.144	0.144	0.138	0.145	0.142	0.134	0.129	0.117	0.110	0.0974
T_M/%	61.74	59.76	58.09	52.31	60.54	57.57	55.44	60.55	54.10	54.71
R_0/µm	15.11	20.14	25.18	30.21	35.25	40.29	45.32	50.36	55.39	60.43
R_f/µm	267.04	201.04	161.96	136.73	119.60	107.80	99.78	94.53	91.42	89.98
f_d/cm	13	14	15	16	17	18	19	20	21	22
N_M/%	0.0951	0.0829	0.0763	0.0760	0.0662	0.0609	0.0579	0.0574	0.0501	0.0474
T_M/%	58.38	53.46	56.10	53.17	51.21	55.68	50.11	55.71	54.93	55.10
R_0/µm	65.46	70.50	75.53	80.57	85.61	90.64	95.68	100.71	105.75	110.78
R_f/µm	89.58	90.75	92.46	94.82	97.69	100.95	104.53	108.36	112.40	116.60

where

A_1	0.1505
A_2	0.04719
x_0	12.4206
dx	2.9249
Correlation coefficient (r^2)	0.9920

The dispersion observed in Fig. 7B, similar to that observed in Fig. 6B, seems to show the absence of a mathematical relationship between the averaged transmittances of the maxima and the focal length.

3.3. Influence of the prefocused radius

The simulations performed in this case were characterised by the data listed below.

Wavelength (λ/nm)	632.8
Focal length (f_d/cm)	10
Range of evaluated prefocused radii (r/µm)	200–1150

The He–Ne laser wavelength (632.8 nm) has been used for the same reason explained in the previous section describing the study of the influence of the focal length.

In Table 4 are listed the data of maximum noise, which are plotted versus r in Fig. 8. Fig. 8A shows how the noise increases when r grows and how the noise stays at an almost constant value when r takes higher values. This behaviour fits in good agreement with

$$y = \frac{ABx^c}{1 + Bx^c} \tag{7}$$
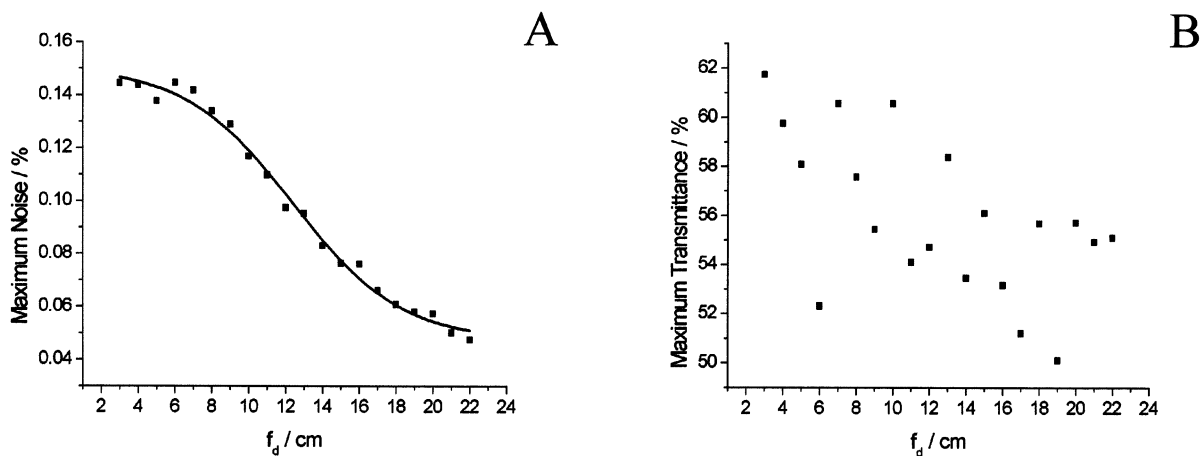
Fig. 7. Plots of data corresponding to the maximum noise reached in the tests for the study of the influence of f_d: A, maximum noise versus f_d; B, maximum transmittance versus f_d.

Table 4

Transmittances (T_M) and associated noise (N_M) corresponding to the points of maximum noise reached in the simulated processes performed to evaluate the influence of r. These points have been calculated using the best fifth-order polynomial fit. The radius of the focus (R_0) and the radius of the path at the photoreceptor plane (R_f) are also shown

$r/\mu m$	200	250	300	350	400	450	500	550	600	650
$N_M/\%$	0.0487	0.0708	0.0934	0.102	0.117	0.125	0.135	0.138	0.136	0.135
$T_M/\%$	53.15	51.26	56.80	57.88	60.04	55.15	60.35	56.35	57.39	52.94
$R_0/\mu m$	100.71	80.57	67.14	57.55	50.36	44.76	40.28	36.62	33.57	30.99
$R_f/\mu m$	108.36	94.82	90.04	90.62	94.53	100.52	107.82	115.92	124.61	133.64
$r/\mu m$	700	750	800	850	900	950	1000	1050	1100	1150
$N_M/\%$	0.139	0.139	0.145	0.147	0.153	0.155	0.150	0.150	0.151	0.136
$T_M/\%$	65.60	56.77	58.01	59.89	59.97	59.39	65.10	56.20	58.46	62.47
$R_0/\mu m$	28.77	26.86	25.18	23.70	22.38	21.20	20.14	19.18	18.31	17.52
$R_f/\mu m$	142.95	152.37	161.96	171.62	181.39	191.20	201.04	210.91	220.78	230.60

where

A	0.1509
B	1.403×10^{-7}
c	-1.8386
Correlation coefficient (r^2)	0.9754

Finally, the graphs in Fig. 8B, similar to Fig. 6B and Fig. 7B, seems to confirm the absence of a mathematical relationship between the transmittances of the maximums and r.

3.4. Focused paths and radial parameters

The mathematical relationships found in the noise in connection with changes in some of the focal parameters λ, f_d or r (Figs 6A, 7A and 8A) confirm the presence of a link between noise and the dimensional features of the focused path. In qualitative terms, this dependence can be explained in relation to the changes undergone by the radial parameters, R_0 and R_f, when some of the focal parameters vary.

The smallest radius in a focused path is that of the focus, R_0. Since the particles have radii of the same order, their presence in positions close to the focal region could bring about partial or total eclipses. It is obvious that the smaller the radius of the focus, the stronger the probability of total or major eclipses. This means that the dynamics of the system would cause strong oscillations in the transmittances, whose associated noise would be large as the value of R_0 is small.

The other parameter used for characterising the focused path is R_f. As can be seen from Fig. 9, its magnitude is equivalent to the angle of the asymptotic cone (Θ). A high value of R_f means that the radius of the focused path increases rapidly from the focal region to the position occupied by the photoreceptor unit. However, when R_f is small, the influencing focal region is longer and, for that reason, it is more likely to experience major eclipses. Hence we can conclude that the smaller the value of R_f, the stronger will be the noise associated with the transmittance of a precipitant system.
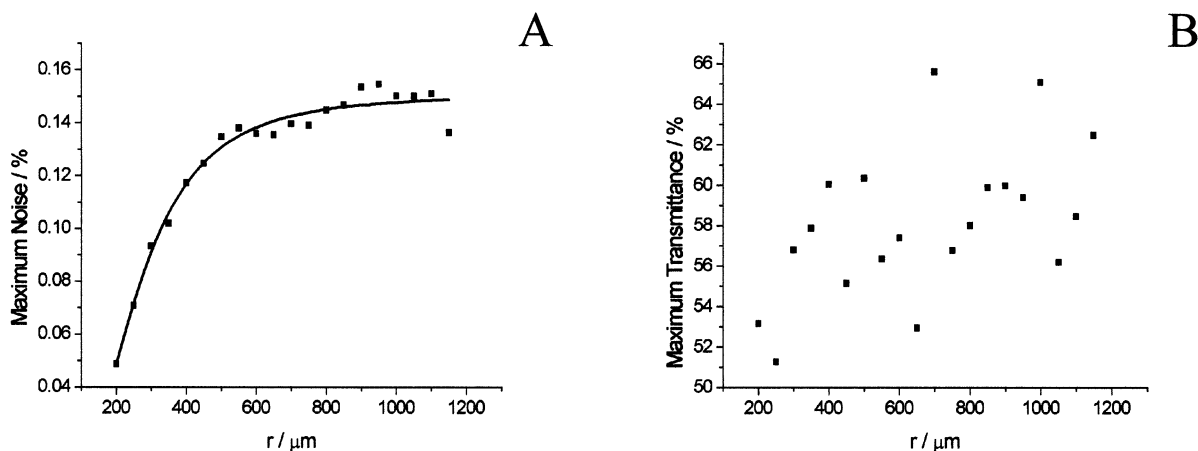
Fig. 8. Plots of data corresponding to the maximum noise reached in the tests for the study of the influence of r: A, maximum noise versus r; B, maximum transmittance versus r.
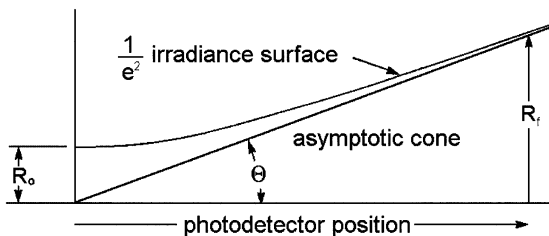
Fig. 9. Schematic illustration showing the parameters R_0 and R_f in a focused path.

Fig. 10 shows the variation in the values of R_0 and R_f in relation to changes in λ. The linear increase observed in both radial parameters justifies the curve shown in Fig. 6A, where a linear decrease can be seen.

In the range of the evaluated focal lengths, the changes observed in R_0 (Fig. 11A) also establish a linear increase which is in accord with the generalised decrease of noise shown in Fig. 7A. However, changes in R_f are of a different nature. The curve shown in Fig. 11B, displays a first section of strong decrease and a second section of steady, smooth increase. According to this, the evolution of R_0 and R_f shows opposite tendencies in focal lengths from 3.0 cm to the minimum of the curve in Fig. 11B, situated at 12.6 cm, and equal tendencies from this value up. The inflexion point of the curve shown in Fig. 7A, situated at 12.4 cm and calculated by Eq. (6), illustrates this change of tendency.

Finally, Fig. 12 shows the changes in R_0 and R_f, in the range of the evaluated values of r. It can be observed that the higher the value of r, the smaller the value of R_0. The effect caused by this variation involves a progressive increase in the values of maximum noise that seems to be proportional to the slopes of the curve in Fig. 12A at each point.
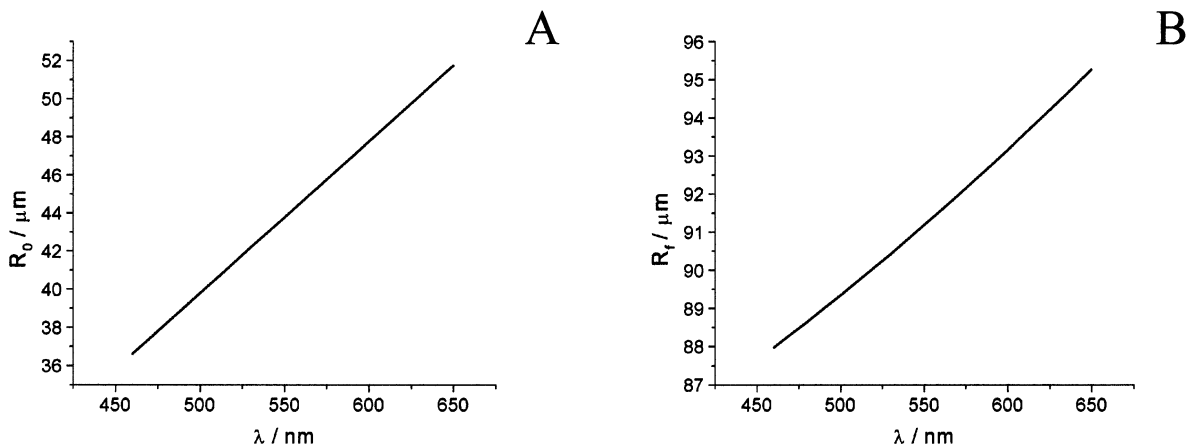
Fig. 10. Plots of R_0 and R_f values in focused paths obtained using data of wavelengths ranging from 460 to 650 nm.
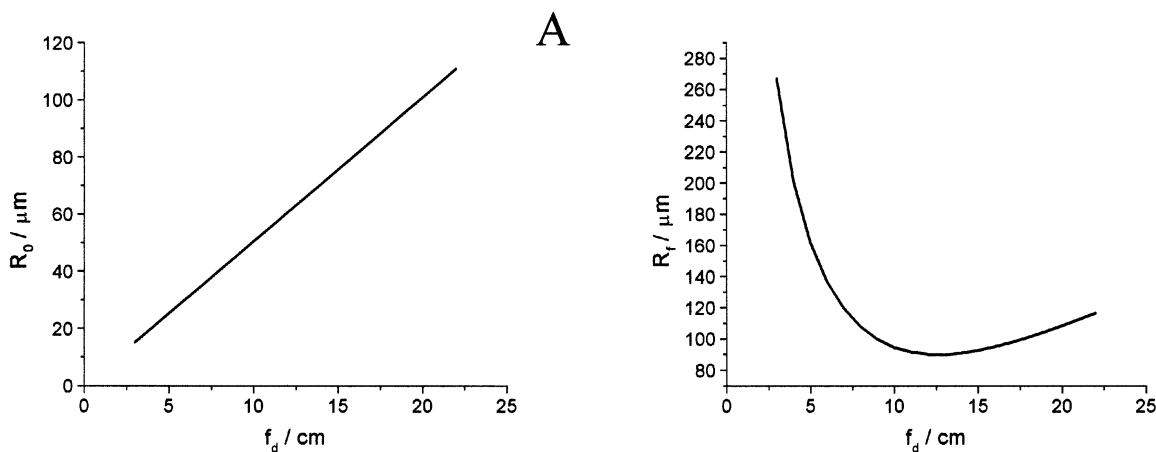
Fig. 11. Plots of R_0 and R_f values in focused paths obtained using data of focal lengths ranging from 3 to 22 cm.
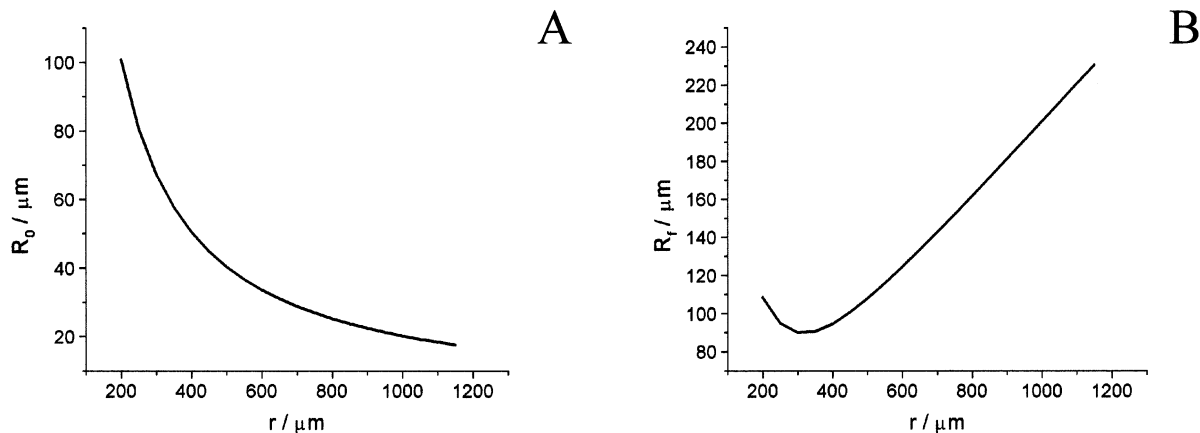
Fig. 12. Plots of R_0 and R_f values in focused paths obtained using data of prefocused radii ranging from 200 to 1150 μm.

On the other hand, variations of R_f show opposite trends. From $r = 200.0$ μm to the position of the minimum of the curve in Fig. 12B, placed at 317.4 μm, the progressive decrease found creates an effect additional to that caused by the variation of R_0. However from this value up, R_f shows an increase that affects maximum noise in an opposite way. As a whole, the evolution of the radial parameters justifies the evolution of the values of maximum noise shown in Fig. 8A.

The first section of increasing noise that can be observed in Fig. 8A is in accord with the same tendencies shown by both radial parameters. The second section shows a stabilisation of noise around a constant level, reached by compensation of the effects caused by the decrease of the slope of the curve in Fig. 12A and the substantial increase of R_f (Fig. 12B).

3.5. Comments on the numerical range of the focal parameters

Once focused paths and radial parameters have been evaluated, it is convenient to point out some details related to the range of values that have been found for R_0 and R_f. They are shown in Table 5 together with values of λ, f_d and r.

The ranges corresponding to f_d and r are much wider than that of λ. For that reason, it must be taken into consideration whether the linear relation shown by the terms of maximum noise in Fig. 6A could be a consequence of the narrow range of λ evaluated. To solve this question it is necessary to test a wider range, however this study has not been developed because the additional values would be out of the visible spectrum range, which goes beyond the scope of this paper.

Table 5
Range of values expressed in μm of the radial parameters (R_0 and R_f) in relation to those of the focal parameters (λ, f_d and r)

	λ	f_d	r
Range of the focal parameter/μm	19.0×10^{-2}	19.0×10^4	95.0×10^1
Range of R_0/μm	15.1	95.7	83.2
Range of R_f/μm	7.3	177.4	140.6

Changes in f_d and r, give rise to greater variations in the radial parameters. The range of values used in this case was wide enough to obtain deeper knowledge of their influence in relation to λ.

References

Apostol T.M. (1967). Calculus, Vol. 1, Wiley.

Gerrard A. & Burch J.M. (1994). Introduction to Matrix Methods in Optics. Dover Publications, New York.

Martín J., Alcántara R. & García-Ruiz J.M. (1991). Cryst. Res. Technol. 26, 35.

Martín J., García-Ruiz J.M. & Alcántara R. (1992). Cryst. Res. Technol. 27, 799.

Poce-Fatou J.A., Alcántara R., Gallardo J.J. & Martín J. (2000). Comput. Chem. in press.